Water and Environmental Sustainability (WES)
ISSN: 2710-3404
DOI: 10.52293/WES.3.3.110
H o m e p a g e: https://www.journalwes.com/

Podcasts

ORIGINAL RESEARCH PAPER

Superhydrophobic Surface Behaviour of X80 Steel Prepared by Etching Method

Mohd Talha[1], Yangang Jiang1, Xiaohong Wang[1*], Hao Liu[1], Shilei Xu[1], Yuanhua Lin[1,2]

1. School of New Energy and Materials, Southwest Petroleum University, Chengdu, 610500, Sichuan, P.R. China
2. State Key Laboratory of Oil and Gas Reservoir Geology and Exploitation, Southwest Petroleum University, Chengdu 610500, Sichuan, P. R. China.

A R T I C I E I N F O

Keywords:
Superhydrophobic
X80 steel
Micro/nano Structure
Anti-wax Properties
SEM

Corresponding Author:
869258280@qq.com

Article History:
Received: 20 Nov, 2022
Revised: 24 Jan, 2023
Accepted: 31 Jan, 2023

A B S T R A C T

In order to solve the corrosion and wax deposition problem of X80 steel used in oil pipelines, a hydrophobic surface layer was prepared by ferric chloride pre-etching followed by hydrochloric acid etching and finally surface modification with fluorosilane. The study revealed that the best hydrophobic effect was obtained when the concentration of ferric chloride was 0.21 g/ml, the concentration of hydrochloric acid was 1.5mol/L, and the etching time was 30min. The X80 steel etched with the above process has excellent hydrophobicity and demonstrated a contact angle value of 158º and only change to 150º even exposed to air for three months. The X80 steel etched with the above process also has anti-waxing properties and the wax-proof rate was more than 66%. The corrosion resistance properties of such formed surfaces of X80 steel was also analyzed by EIS analysis and the results of which demonstrated that the impedance of the etched X80 steel is much higher than that of the non-etched X80 steel. Scanning electron microscopy (SEM) results indicated that the etched X80 steel has excellent anti wax and corrosion resistant properties because of its unique structure, similar to lotus leaf surface, which is comprised of micro and nano pits.

Introduction

In recent years, high-strength X80 steel pipelines has been rapidly developed in crude oil transportation. By 2019, the X80 steel pipelines, being the most widely used high-strength pipeline steel and have exceeded to 30,000 kms worldwide(Yi Shuai, Xin-Hua Wang, Y.Frank Cheng. Buckling resistance of an X80 steel pipeline at corrosion defect under bending moment. Journal of Natural Gas Science and Engineering, 93, 104016, 2021., Zhang SZ, Cheng YF, Feng XD. Performance characteristics and technical challenges of X80 pipeline steel. J. Oil. Gas. Storage Trans. 38, 481- 495, 2019.).

The crude oil usually contains 5 to 30 wt% of n-paraffin or n-alkanes with 18 to 65 carbon atoms(X.P. Zhang, F. Yang, B.Yao, C.X. Li, D.W. Liu, G.Y. Sun. Synergistic effect of asphaltenes and octadecyl acrylate-maleic anhydride copolymers modified by aromatic pendants on the flow behavior of model waxy oils. Fuel, 260(116381), 2020.). The high amount of paraffin generally leads to the deposition of paraffin on the pipeline surface when the temperature is lower than the wax appearing temperature (WAT) of crude due to the supersaturation of wax crystals(Ashish Dewangan, Ashok Kumar Yadav. Wax deposition during production of waxy crude oil and its remediation,

Petroleum Science and Technology, 2017(35):18, 1831-1838., Gang Chen, Jiao Lin, Weimin Hu, Chao Cheng, Xuefan Gu, Weichao Du, Jie Zhang, Chengtun Qu. Characteristics of a crude oil composition and its in situ waxing inhibition behavior. Fuel, 218(2018): 213-217. , Jun Xu, Shili Xing, Huiqin Qian, Sheng Chen, Xiaoming Wei, Rui Zhang, Li Li, Xuhong Guo, Effect of polar/nonpolar groups in comb-type copolymers on cold flowability and paraffin crystallization of waxy oils, Fuel, Volume 103, Pages 600-605, 2013., Kaifeng Fan, Si Li, Rongbin Li. Development of wax molecular diffusivity correlation suitable for crude oil in wax deposition: Experiments with a cold-finger apparatus. Journal of Petroleum Science and Engineering, 205(2021)108851.). The deposition of paraffin during crude oil transportation increases pumping costs and hinders the flow of the pipeline and also leads to pipeline corrosion. In extreme scenarios, wax deposition may lead to a complete blockage of the pipe(Yun Lei, Pengfei Yu, Wenqiang Ni, Haoping Peng, Yang Liu, Xiaofang Lv, Huijun Zhao. Study on the Kinetic Process of Asphaltene Precipitation during Crude Oil Mixing and Its Effect on the Wax Behavior of Crude Oil. ACS Omega 2021, 6, 1497−1504.). Hence, the oil industries are facing billions of losses every year (Hamid O. Bidmus, Anil K. Mehrotra. Solids Deposition during “Cold Flow” of Wax−Solvent Mixtures in a Flow-loop Apparatus with Heat Transfer. Energy Fuels, 2009, 23(6), 3184- 3194., Himani Negi, Sundram Sharma, Raj K. Singh. Assessment of cellulose substituted with varying short/long, linear/branched acyl groups for inhibition of wax crystals growth in crude oil, Journal of Industrial and Engineering Chemistry, 104(2021), 458-467., L. F. A. Azevedo, A. M. Teixeira. A Critical Review of the Modeling of Wax Deposition Mechanisms. Petroleum Science and Technology, Volume 21, 2003, Issue 3-4.).

Numerous methods have been reported for managing and suppression wax deposition problems at industrial scale(Haoran Zhu, Chuanxian Li, Zongming Xiu, Zhiqiang Zhao, Kai Mu, Hui Dai, Feng Wang, Fei Yang, and Bo Yao. Effect of Ethylene-Vinyl Acetate Copolymer/Amino-Functionalized Polymethylsilsesquioxane Composite Wax Inhibitor on the Rheological and Wax Depositing Characteristics of Waxy Crude Oil. Energy Fuels, 2020, 34, 8120-8128., Letícia Steckela, Rita C.P. Nunes, Paulo C.S. Rocha, Antônio C.S. Ramos, Dellyo R.S. Alvares, Elizabete F. Lucas. Pour point depressant: identification of critical wax content and model system to estimate performance in crude oil. Fuel, 307(2022) 121853., Xuedong Gao, Qiyu Huang, Xun Zhang, Weidong Li, Yu Zhang, Rongbin Li, and Ruiqi Chen. Estimating Wax Plug Transportation Force in Crude Oil Pipeline Pigging. Energy Fuels, 2020, 34, 3110-3120.). The oil industries presently use costly and complex methods, including mechanical (pigging), chemical, and thermal methods, to prevent wax deposition. As interest is growing in preventive methods, to impede the deposition and reduce the number of well interventions and shut-downs(Davila FG, Silva CMF, Steckel L, Ramos ACS, Lucas EF. Influence of asphaltene aggregation state on the wax crystallization process and the efficiency of EVA as a wax crystals modifer: a study using model systems. Energy Fuels 2020; 34(4): 4095-105., Hao LZ, Al-Salim HS, Ridzuan N. A review of the mechanism and role of wax inhibitors in the wax deposition and precipitation. Pertanika J Sci Technol 2019; 27 (1): 499- 526.), preparation of superhydrophobic (contact angle(CA) > 150°) and oleophobic coating on the inner wall of the pipeline has become a hot research topic. It is an effective way to manage corrosion problem and wax deposition inside crude oil pipeline by preparing superhydrophobic coating with good anti-wax performance(Zhiwei Wang, Liqun Zhu, Huicong Liu, Weiping Li. A conversion coating on carbon steel with good anti-wax performance. Journal of Petroleum Science and Engineering 112 (2013) 266–272.). Superhydrophobic-oleophobic coating can meet both requirements of anti-corrosion as well as anti-waxing and has a huge application prospect in long-distance pipelines. Among many superhydrophobic coatings, the preparation process of fluorosilane modified coating is relatively better and has been widely studied. Cai(Ying Cai, Jing Li, Lingmin Yi, Xiaojie Yan, Jiawei Li. Fabricating superhydrophobic and oleophobic surface with silica nanoparticles modified by silanes and environment-friendly fluorinated chemicals. Applied Surface Science, 450(2018) 102-111.) obtained superhydrophobic and oil-repellent coating surface by using silica co-modified by methyltrimethoxysilane and 1H,1H,2H,2H-perfluorooctyltriethoxysilane, the water contact angle of the coating could reach 150.2°. Pei(Mingliang Pei, Lixia Huo, Xiaomei Zhao, Shuzhen Chen, Jiaxin Li, Zixin Peng, Kaifeng Zhang, Hui Zhou, Peng Liu. Facile construction of stable hydrophobic surface via covalent self-assembly of silane-terminated fluorinated polymer, Applied Surface Science, 507(2020) 145138.) developed a facile strategy to construct stable hydrophobic surface via the covalent self-assembly of silane-terminated fluorinated polymer as surface-attached polymer, which provided a universally applicable coating

technique for the stable hydrophobic surface on various substrates. However, the complex preparation process and high cost limits the application of such coatings.

In this work, based on low-cost pre-etching method, a fluorosilane modified superhydrophobic surface coating was prepared on the surface of X80 steel by ferric chloride pre-etching followed by hydrochloric acid etching and surface modification with fluorosilane. Then, the surface properties and morphology, water contact angle, composition and corrosion resistance of superhydrophobic coating were studied respectively by scanning electron microscope (SEM), contact angle measurement, X-ray diffraction (XRD) and electrochemical impedance spectroscopy (EIS) analysis. This work could provide a new strategy to fabricate hydrophobic/oleophobic surface for inner wall of crude oil pipeline.

Experimental method

Sample preparation and etching process

The material used in this study is a commercially available X80 steel, whose composition is shown in Table 1. It was processed into a plurality of block samples having a size of 30 mm × 20 mm × 2 mm having a hole with diameter of 3mm at one end, and the surface of the sample was first polished with emery paper from 200# to 1200# sequentially. The surface of the sample was then washed with deionized water, then ultrasonically cleaned with ethanol, and dried before each experiment.

Table 1. Chemical compositions of X80 pipeline steel (wt.%)

Elements Content	C	Si	Mn	P	S	Ni	Cr	Cu
	0.0466	0.204	1.754	0.0082	0.0009	0.206	0.235	0.174
	Nb	V	Ti	Mo	Al	B	Fe	
	0.0524	0.022	0.0142	0.125	0.0265	0.004	Balance	

Prepared specimens were hanged in FeCl3 solution with concentration of 0.17g/ml, 0.19g/ml, 0.21g/ml, 0.23g/ml and 0.25g/ml and pre-etch them at room temperature for 5 minutes, then immerse them in HCl solution of 0.5 mol/L, 1mol/L, 1.5mol/L, 2mol/L, 2.5mol/L and 3mol/L, and etch them at room temperature for 10, 20, 30, 40 and 50 minutes. After etching, samples were washed with deionized water and dried in air. Then the etched samples were immersed in 1% fluoroalkylsilane(1H, 1H, 2H, 2H perfluorodecyl triethoxysilane)-ethanol solution at room temperature for more than 30 minutes, then washed with ethanol and deionized water respectively, and finally dried at 60 ºC under drying chamber for 10 minutes. The experimental process for preparing superhydrophobic surface of X80 steel is shown in Fig.1.

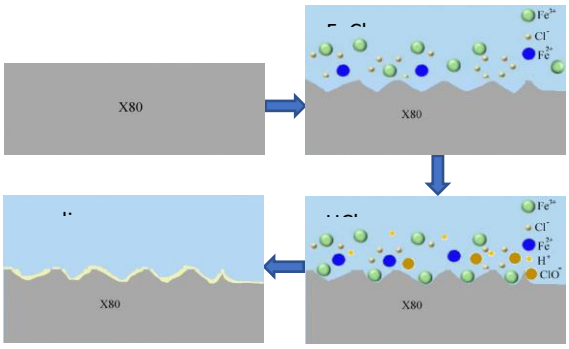

Fig. 1 Schematic diagram of preparation process of superhydrophobic surface of X80 steel

Characterization of Surface Structure of X80 Steel after Etching

SEM analysis

The surface structure of etched X80 steel was analyzed by SEM (ZEISS-EV0-MA15).

XRD analysis

The phase analysis of the material was carried out by DX-1000 X-ray diffractometer. The scanning speed was 4°/min and the scanning range was 5°-80°.

Contact angle measurement

The contact angle (CA) of water droplets on the surface was measured by L-18 contact angle measuring instrument. The volume of water droplet was 5 µL. The rolling angle of water droplets was measured by L-1 rolling angle measuring instrument. The contact angle data were obtained from the average of six recordings under identical conditions and using the best picture.

EIS analysis

EIS analysis was performed using the AUTOLAB PGSTAT302N electrochemical workstation of X80 steel samples before and after etching. The instrument has three-electrode cell assembly, in which the saturated calomel electrode was used as reference electrode and the platinum electrode was used as counter electrode. The samples were the working electrode with exposed area of 1 cm2. 3.5 wt.% NaCl was used as test solution. Before EIS, samples were dipped in test solution for 1 h to get stable open circuit potential. EIS analysis was studied

in the range from 105 to 10-2 Hz with amplitude of 10 mV using an AC signal at open circuit potential. The impedance data were analyzed to assess the corrosion characteristics. ZSimpWin software was used to simulate the experimental EIS data. All the measurements were done thrice and the average values are reported using the best figures. A fresh solution was used for every electrochemical experiment.

Wax resistance test

Anti-wax performance was tested with the device as shown in Fig.2 to compare the anti-wax effect of X80 steel samples before and after etching. Crude oil used in Anti-wax performance test was collected from North west oil field in China and the main characteristics of the crude oil are listed as follows: wax 4.5% wt.%, water 40 wt.%, WAT 23 ºC, pour point 4º C. The samples of X 80 steel before and after etching having a size of 25mm × 16mm × 2mm were suspended in the beaker containing crude oil. The beakers were heated to 80 ºC with a digital display water bath of model HH-type and samples were kept at this temperature for 30 minutes. After that, the beaker was transferred to another water bath of model HHWO-type digital water bath and cooled to 3 ºC for 2 hours. The samples were taken out from beaker and rinsed with deionized water to remove the crude oil on the surface of the samples. The wax deposition test was repeated three times for both etched and blank surface (X80 steel without etched). Wax deposition weight was measured with electronic balance. Macrographs of specimens before and after the test were obtained by a digital camera.

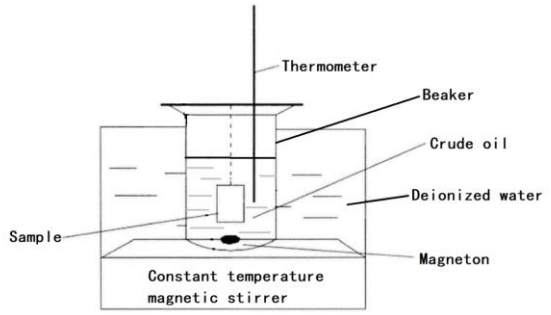

Fig. 2. Schematic diagram of wax resistance test device

Results and discussion

SEM analysis

Fig.3 shows the surface of the abraded and after etching of the X80 steel samples at different magnifications. It can be seen that both the surfaces are significantly different. There are many pits with a diameter of about 20µm on the etched surface. Fig.3c and Fig.3d shows magnified image of pits for better observation of the etched material surface structure. It can be seen that a cluster of layered structures distributed inside the pit. These layered structures can effectively capture air and form an air cushion, so that the water droplets cannot contact with the base completely on its surface, but some of the water droplets contact with the surface, thus showing good hydrophobicity. The nesting of pits and fine layered structures results in the micro-nano composite structure on the surface of X80 steel, and this micro-nano structure is one of the important reasons for the superhydrophobic properties of the steel sheet surface.

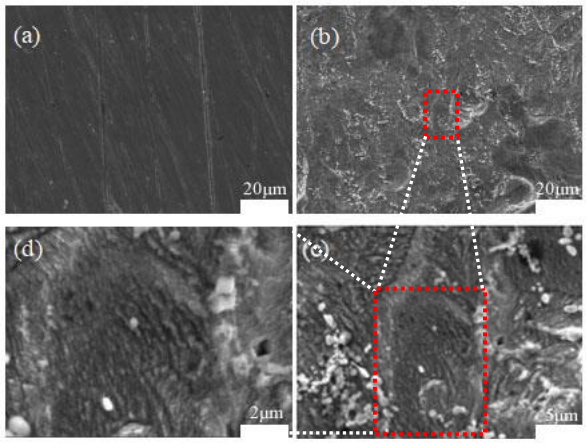

Fig. 3 SEM image of X80 steel surface before and after etching

Fig. 3: SEM image of polished and etched X80 steel surface: (a)500x magnification of the surface topography of the polished sample, (b)500x magnification of the surface topography of the etched sample, (c) 2000x magnification of the surface topography of the etched sample, (d)5000x magnification of the surface topography of the etched sample

XRD analysis

Fig.4 shows the XRD patterns of X80 steel sample without etching, etched sample and fluoroalkylsilane modified steel sample. According to the diffraction peaks, the crystal peaks at the scanning angle of 2θ at 44.675, 65.026 and 82.339° are the diffraction peaks of (110), (200) and (211) crystal planes of iron-based metals, respectively. Comparing the blank sample with the etched sample, it can be seen that the etched sample maintains the

diffraction characteristics of the iron matrix, which indicates that the crystal structure of the iron matrix is not damaged during the etching process. Comparing the XRD patterns of the blank sample and the sample modified by fluoroalkylsilane, it can be seen that the diffraction peak intensity of the sample modified by fluoroalkylsilane is basically unchanged, which indicates that the deposited fluoroalkylsilane does not change the unit cell structure of the matrix.

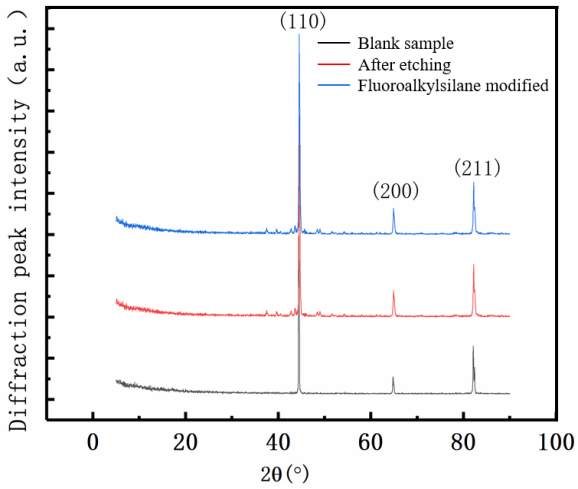

Fig. 4 XRD pattern of X80 steel before and after etching

Contact angle

Fig.5 shows the effect of FeCl3 concentration on contact angle of X80 steel after etching. It can be seen that the contact angle after etching increases first and then decreases with the increase of the concentration of FeCl3 and when the concentration is 0.21g/ml, the contact angle of X80 steel reaches the maximum value of 158.2±2°. The reason for this is as follows: The hydrophobicity of etched X80 steel is affected by its surface roughness and the surface roughness is affected by reaction rate of different micro areas. The low concentration FeCl3 solution results in low reaction rate, making the surface of X80 steel have inadequate roughness after pre-etching, while the high concentration solution will make the surface of the sample over etched, causing the generated microstructure to be destroyed, and also can't get enough roughness. When pre-etching time is 5mins, the concentration of FeCl3 is 0.21 g/ml, the pre-etched sample can have proper roughness, which leads to high contact angle.

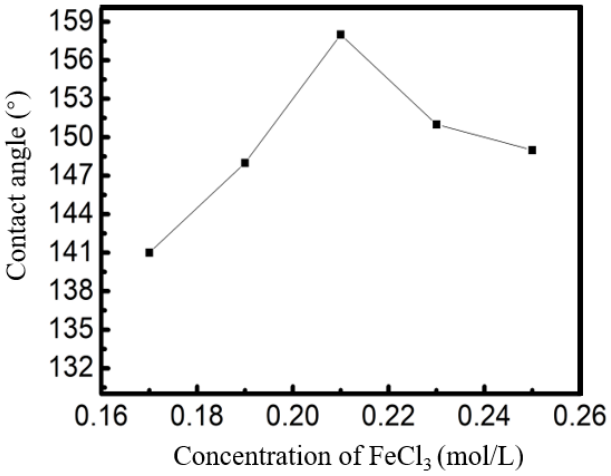

Fig. 5 Effect of FeCl3 Concentration on Water Contact Angle

Fig.6 shows the photograph of the contact angle of X80 steel after etching with different concentrations of HCl solution for 30 minutes and the effect of HCl concentration on the surface wetting properties of X80 steel is shown in Fig.7. The contact angle of water droplets on the surface of X80 steel increases gradually with the increase of HCl concentration and the maximum contact angle obtained was158°±2° when the concentration of solution is 1.5mol/L, but as the concentration increase further, the contact angle decreases. The possible reason is also because the corrosion rate difference between the fine ferrite and the grain boundaries reached a suitable level and the contact angle of the etched X80 steel reached at maximum when HCl concentration was 1.5 mol/L. As can be seen from the SEM image, the surface morphology featured flake-like nano structures with some grooves. In general, there was an increase in the height and density of flake-like structures with increased etching solution concentration. As the concentration increased from 0.5 mol/L to 1.5 mol/L, the grooves became larger, forming hierarchical micro/nano structures. With further increase of etching solution concentration, the structure showed partial damage. Consequently, the etching morphology of 2 mol/L HCl etched surface and 2.5 mol/L HCl etched surface became flatter, which leads to the decrease in the contact angle.

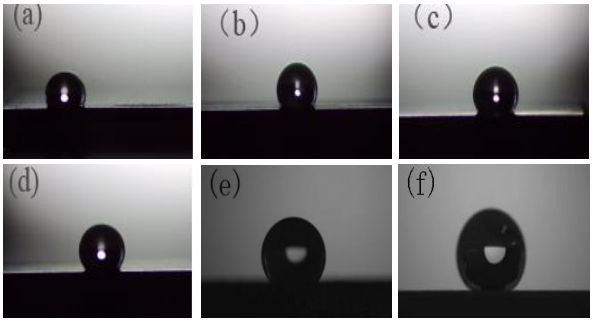

Fig. 6 Contact angle of steel sheet etched with different concentrations of HCl, (a) 0.5mol/L HCl; (b) 1mol/L HCl; (c) 1.5mol/L HCl; (d) 2mol/L HCl; (e) 2.5mol/L HCl; (f) 3mol/L HCl.

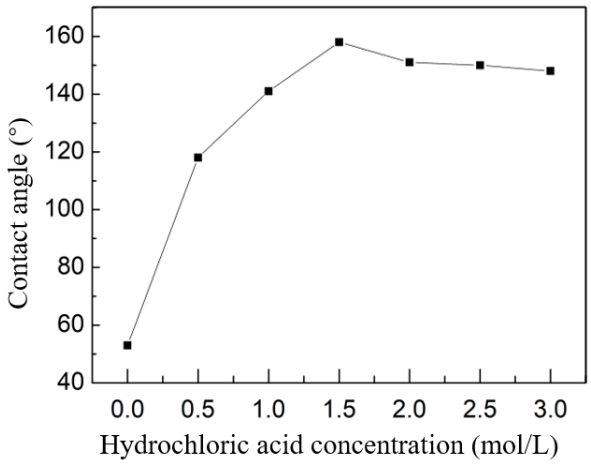

Fig. 7 Effect of HCl concentration on contact angle

Fig. 8 shows the water contact angle under different etching time using 1.5 mol/L HCl solution and Fig.9 shows the influence of etching time on wettability of X80 steel surface. It can be seen from Fig.9 that as the etching time increase, the contact angle of the X80 steel etched increased continuously. When the etching time is 30 minutes, the contact angle of the etched X80 steel reaches a maximum value of 158°±2°. The water contact angle decreases after further increasing etching time and eventually tends to reach a certain value. The reason is as follows: the roughness of the X80 surface on the micro and nanoscale increases with etching time because corrosion rate difference between the fine ferrite and the grain boundaries and gradually formed a micro-bulge on the X80 surface after a certain etching time. When these micro-bulges are further etched, the roughness of the X80 steel gradually decrease which reduces the contact angle.

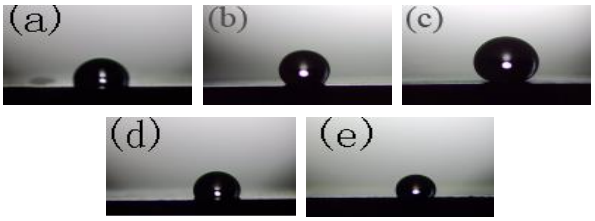

Fig. 8 Surface of X80 steel sheet with different etching time; (a) etching for 10 min; (b) etching for 20 min; (c) etching for 30 min; (d) etching for 40 min; (e) etching for 50 min

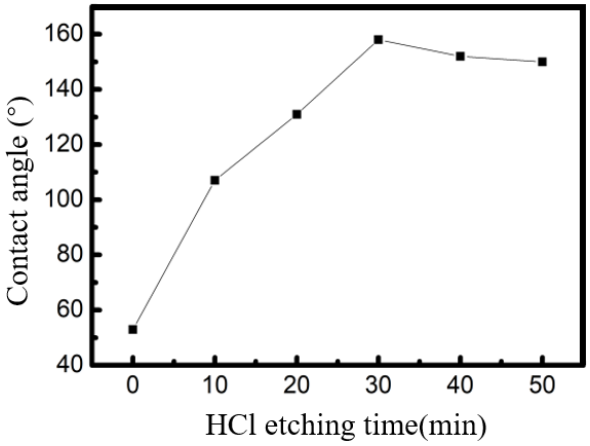

Fig. 9 Effect of HCl etching time on water contact angle

Fig.10 shows the contact angle of the etched X80 steel exposed to air for three months. It can be seen from the figure that the contact angle of etched X80 steel after three months is still large i.e. 150°±2°, which is only 5% lower than the contact angle of the sample just after preparation. Thus, superhydrophobic surface prepared by the two-step etching method has good stability.

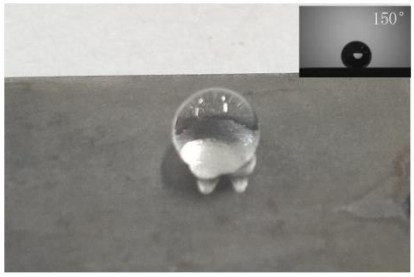

Fig. 10 contact angle of the X80 steel surface exposed to air for three months

EIS analysis

Fig.11 shows the Nyquist plots of polished and modified superhydrophobic X80 steel samples in 3.5 wt.% NaCl solution. As can be seen from the figure, the prepared superhydrophobic X80 steel has

excellent corrosion resistance, and the impedance is up to 106 orders of magnitude, which is much larger than the impedance of the unetched X80 steel sample.

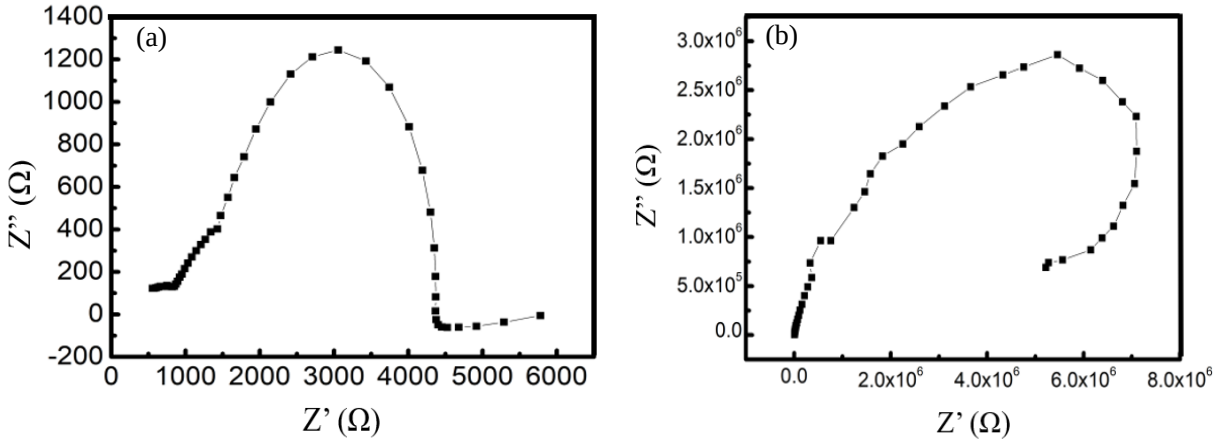

Fig. 11 Nyquist plots of X80 steel in 3.5 wt.% NaCl; (a) blank sample and (b) superhydrophobic

The electrochemical parameters obtained by fitting the EIS data using equivalent electric circuits (Fig.11 (a) & (b)) are shown in Table 2. It can be seen that the solution resistance Rs of the superhydrophobic sample is much larger than that of the blank sample, which is about 6 times of that of the blank sample. From the value of the charge transfer resistance (Rct), it can be seen that the Rct of the superhydrophobic sample increases from 3254 ohm to 62650ohm, which indicates that the superhydrophobic sample has good corrosion resistant property. As shown above, both microrods and nanosheets are present at the prepared superhydrophobic surface, entrapping a mass of air and thus a capillary system forms on the rough surface. When the solution comes in contacts with surface, it would repelled by the driving force derived from the difference in pressure. Consequently, it is hard for the corrosive ions to reach the superhydrophobic surface, which significantly improves the corrosion resistance of superhydrophobic surfaces.

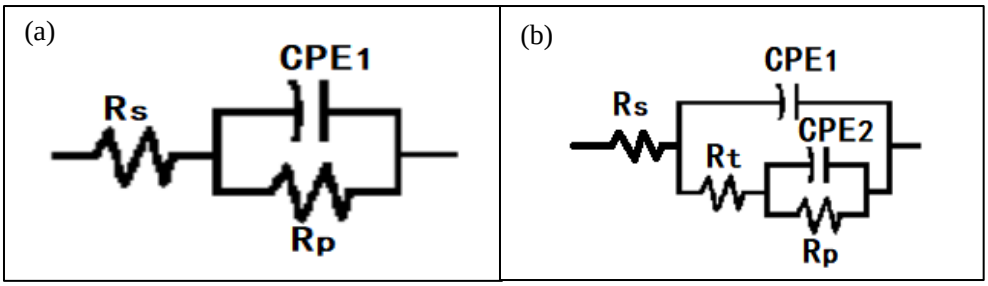

Figure 12: Equivalent circuit diagram of (a) blank sample and (b) superhydrophobic sample

Table 2 Impedance spectrum fitting parameters of blank sample and superhydrophobic sample

Sample	Rs/ohm	CPE1/F	Rt/ohm	CPE2/F	Rct/ohm
Blank	995	6.961×10-6	-	-	3254
superhydrophobic	6344	5.285×10-6	1.031×104	1.941×10-5	6.265×104

Anti-wax Analysis

silver color with metal luster as shown in Fig.13a, while a layer of black wax deposits on the X80 steel after immersion in the crude oil with a wax

The anti-wax test was carried out and the results are shown in Fig.13. The X80 steel before the test has

content of 4.5% as shown in Fig.13b. In comparison to the polished sample, the etched samples have better anti-wax performance. As indicated in Fig.13c and

Fig.13d, the etched X80 steel is uniformly gray and has a little wax deposited after immersion in the crude oil with wax content of 4.5%. The reason is that a layer of fluoroalkylsilane is deposited on the surface of the sample, which has low surface tension and reduces the adhesion between the inner wall of the pipeline and the wax, so that the wax deposited on the etched X80 steel samples reduces with a small shear force, so as to achieve the purpose of preventing wax deposition. The reason for this phenomenon may be that the van der Waals interaction between the long chains of the fluoroalkyl silane modifier molecules is strong, showing an increased predisposition to self-organize, thereby reducing the adhesion of the sample surface to the wax. In fluoroalkyl, the fluorine atom has a larger radius compared to the hydrogen atom, and there is a dipole-dipole interaction between the alkyl chains that contain fluorine atoms, so the presence of the fluorine atom also reduces the surface of the hydrophobic and oleophobic surface free energy.

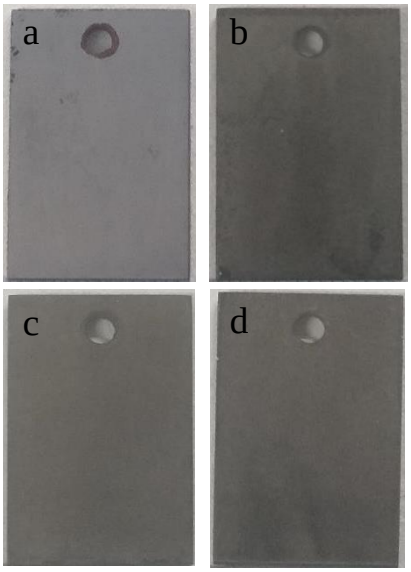

Fig. 13: Surface of X80 steel sheet before and after immersion in the crude oil with a wax content of 4.5% (a) blank sample before being immersed (b) blank sample after 2 hours of immersion (c) X80 steel sheet etched before being immersed (d) X80 steel sheet etched after 2 hours of immersion

The wax deposition weight of X80 steel without etching is 945 mg in average and the wax deposition weight of X80 steel etched is only 321 mg in average. According to the calculation result of equation (i), the anti-wax effect can be quantitative evaluated and the Anti-wax rate of etched sample was found to be 66%.

$$P_R = (W_1 - W_2)/W_1 \times 100\% \quad \text{(i)}$$

where, PR represents anti-wax rate, W1 represents wax deposit on X80 steel sample before etching, W2 represents wax deposit on X80 steel sample after etching.

4. Conclusions

In order to solve the problem of wax deposition on the inner wall of X80 steel in the crude oil pipeline, a two-step etching process, etching in 0.21g/ml FeCl3 solution for 5 minutes, followed by etching in 1.5mol/L HCl for 30 minutes at room temperature, was used on X80 steel samples and a superhydrophobic and oleophobic surface was obtained with a wax repellency of 66%. The surface contact angle of X80 steel prepared by the optimized etching process is 158±2°. After exposure to air for 3 months, the surface contact angle decreases by only 5%, which exhibits good stability of superhydrophobic surface. The impedance of X80 steel prepared by the optimized etching process in 3.5% NaCl solution is very high and up to 106 orders of magnitude, which is about 1000 times that of X80 steel without etching. The two-step etching process described in this paper has the advantages of low cost and high efficiency, and can provide solutions for solving the problem of wax deposition in crude oil pipelines.

Declaration of Competing Interest

None.

Acknowledgements

This work was financially supported by the Science & Technology Department of Sichuan Province, No. 2021YJ0346. Authors are also thankful for financial assistance provided by the Sichuan 1000 Talent Fund.

Conflict of interest

The author declare there is no conflict of interest.

References

A. Dewangan, A. K. Yadav, Wax deposition during production of waxy crude oil and its remediation, Pet. Sci. Technol 35(2017) 1831-1838. https://doi.org/10.1080/10916466.2017.1363776.

A. O. Ijaola, P. K. Farayibi, E. Asmatulu. Superhydrophobic coatings for steel pipeline protection in oil and gas industries: A comprehensive review, Journal of Natural Gas Science and

Engineering 83(2020) 103544. https://doi.org/10.1016/j.jngse.2020.103544.

B. Subeshan, R. Asmatulu, Corrosion mitigation of metals and alloys via superhydrophobic coatings with plasma surface and heat treatment processes, Eng. Failure Anal. 139(2022) 106437. https://doi.org/10.1016/j.engfailanal.2022.106437.

E. Zhao, Y. Li, L. Gao, S. Yang, T. Ma, Anti-corrosion properties of a bioinspired superhydrophobic surface on stainless steel, Int. J. Electrochem. Sci. 10(2017) 9855-9864. https://doi.org/10.20964/2017.10.23.

F. G. Davila, C. M. F. Silva, L. Steckel, A. C. S. Ramos, E. F. Lucas, Influence of asphaltene aggregation state on the wax crystallization process and the efficiency of EVA as a wax crystals modifer: a study using model systems, Energy Fuels 34(2020) 4095-4105.
https://doi.org/10.1021/acs.energyfuels.9b04166.

G. Chen, J. Lin, W. Hu, C. Cheng, X. Gu, W. Du, J. Zhang, C. Qu, Characteristics of a crude oil composition and its in situ waxing inhibition behavior, Fuel 218(2018) 213-217. https://doi.org/10.1016/j.fuel.2017.12.116.

H. Negi, S. Sharma, R. K. Singh, Assessment of cellulose substituted with varying short/long, linear/branched acyl groups for inhibition of wax crystals growth in crude oil, J. Ind. Eng. Chem. 104(2021) 458-467. https://doi.org/10.1016/j.jiec.2021.08.043.

H. O. Bidmus, A. K. Mehrotra, Solids Deposition during “Cold Flow” of Wax−Solvent Mixtures in a Flow-loop Apparatus with Heat Transfer, Energy Fuels 23(2009) 3184-3194. https://doi.org/10.1021/ef900224r.

H. Yang, Y. Gao, G. S. Frankel, W. Qin, L. Wu, Robust superhydrophobic surface with reinforced skeletons for corrosion protection, Appl. Surf. Sci. 499(2020) 143916. https://doi.org/10.1016/j.apsusc.2019.143916.

H. Zhu, C. Li, Z. Xiu, Z. Zhao, K. Mu, H. Dai, F. Wang, F. Yang, B. Yao, Effect of Ethylene-Vinyl Acetate Copolymer/Amino-Functionalized Polymethylsilsesquioxane Composite Wax Inhibitor on the Rheological and Wax Depositing Characteristics of Waxy Crude Oil, Energy Fuels 34(2020) 8120-8128. https://doi.org/10.1021/acs.energyfuels.0c00922.

J. Marczak, M. Kargol, M. Psarski, G. Celichowski, Modification of epoxy resin, silicon and glass surfaces with alkyl- or fluoroalkylsilanes for hydrophobic properties, Appl. Surf. Sci. 380(2016) 91-100. https://doi.org/10.1016/j.apsusc.2016.02.071.

J. Xu, S. Xing, H. Qian, S. Chen, X. Wei, R. Zhang, L. Li, X. Guo, Effect of polar/nonpolar groups in comb-type copolymers on cold flowability and paraffin crystallization of waxy oils, Fuel 103(2013) 600-605. https://doi.org/10.1016/j.fuel.2012.06.027.

K. Fan, S. Li, R. Li, Development of wax molecular diffusivity correlation suitable for crude oil in wax deposition: Experiments with a cold-finger apparatus, J. Pet. Sci. Eng. 205(2021) 108851. https://doi.org/10.1016/j.petrol.2021.108851.

L. F. A. Azevedo, A. M. Teixeira, A Critical Review of the Modeling of Wax Deposition Mechanisms, Pet. Sci. Technol 21(2003) 393-408. https://doi.org/10.1081/LFT-120018528.

L. Steckela, R. C. P. Nunes, P. C.S. Rocha, A. C. S. Ramos, D. R. S. Alvares, E. F. Lucas. Pour point depressant: identification of critical wax content and model system to estimate performance in crude oil, Fuel 307(2022) 121853. https://doi.org/10.1016/j.fuel.2021.121853.

M. Pei, L. Huo, X. Zhao, S. Chen, J. Li, Z. Peng, K. Zhang, H. Zhou, P. Liu, Facile construction of stable hydrophobic surface via covalent self-assembly of silane-terminated fluorinated polymer, Appl. Surf. Sci. 507(2020) 145138. https://doi.org/10.1016/j.apsusc.2019.145138.

N. Attarzadeh, M. Molaei, K. Babaei, A. Fattah-alhosseini, New Promising Ceramic Coatings for Corrosion and Wear Protection of Steels: A Review, Surf. Interfaces 23(2021) 100997. https://doi.org/10.1016/j.surfin.2021.100997.

S. Liu, X. Liu, S. S. Latthe, L. Gao, S. An, S. S. Yoon, B. Liu, R. Xing, Self-cleaning transparent superhydrophobic coatings through simple sol–gel processing of fluoroalkylsilane, Appl. Surf. Sci. 351(2015) 897-903. https://doi.org/10.1016/j.apsusc.2015.06.016Get rights and content.

S. Zhao, L. He, X. Fan, C. Liu, J. Long, L. Wang, H. Chang, J. Wang, W. Zhang, Microstructure and chloride corrosion property of nanocrystalline AlTiCrNiTa high entropy alloy coating on X80 pipeline steel, Surf. Coat. Tech. 375(2019) 215-220. https://doi.org/10.1016/j.surfcoat.2019.07.033.

X. Gao, Q. Huang, X. Zhang, W. Li, Y. Zhang, R. Li, R. Chen, Estimating Wax Plug Transportation Force in Crude Oil Pipeline Pigging, Energy Fuels 34(2020) 3110-3120.
https://doi.org/10.1021/acs.energyfuels.9b04466.

X. Zhang, F. Yang, B.Yao, C. Li, D. Liu, G. Sun, Synergistic effect of asphaltenes and octadecyl acrylate-maleic anhydride copolymers modified by aromatic pendants on the flow behavior of model

waxy oils, Fuel 260(2020) 116381. https://doi.org/10.1016/j.fuel.2019.116381.

X. Zhang, J. Zhao, J. Mo, R. Sun, Z. Li, Z. Guo, Fabrication of superhydrophobic aluminum surface by droplet etching and chemical modification, Colloids Surf., A 567(2019) 205-212. https://doi.org/10.1016/j.colsurfa.2019.01.046.

Y. Cai, J. Li, L. Yi, X. Yan, J. Li, Fabricating superhydrophobic and oleophobic surface with silica nanoparticles modified by silanes and environment-friendly fluorinated chemicals, Appl. Surf. Sci. 450(2018) 102-111. https://doi.org/10.1016/j.apsusc.2018.04.186.

Y. Lei, P. Yu, W. Ni, H. Peng, Y. Liu, X. Lv, H. Zhao, Study on the Kinetic Process of Asphaltene Precipitation during Crude Oil Mixing and Its Effect on the Wax Behavior of Crude Oil, ACS Omega 6(2021) 1497-1504. https://doi.org/10.1021/acsomega.0c05121.

Y. S. Bao, W. Wang, B. L. He, M. Wang, Y. Yin, L. Liang, L. Xu, G. Xu, EIS analysis of hydrophobic and hydrophilic TiO2 film, Electrochim. Acta 54(2008) 611-615. https://doi.org/10.1016/j.electacta.2008.07.041

Y. Shuai, X. Wang, Y. Cheng, Buckling resistance of an X80 steel pipeline at corrosion defect under bending moment, J. Nat. Gas Sci. Eng. 93(2021) 104016. https://doi.org/10.1016/j.jngse.2021.104016.

Z. Wang, L. Zhu, H. Liu, W. Li, A conversion coating on carbon steel with good anti-wax performance, J. Pet. Sci. Eng. 112(2013) 266–272. https://doi.org/10.1016/j.petrol.2013.11.013.